Theor Chem Acc (1999) 101:194–204
DOI 10.1007/s00214980m143

Theoretical
Chemistry Accounts

Regular article

Solution conformations of structured peptides: continuum electrostatics versus distance-dependent dielectric functions*

Michael Schaefer[1,2], **Christian Bartels**[2], **Martin Karplus**[1,2]

[1] Laboratoire de Chimie Biophysique, Université Louis Pasteur, Institut le Bel, 4 rue Blaise Pascal, F-67000 Strasbourg, France
[2] Department of Chemistry, Harvard University, 12 Oxford Street, Cambridge, MA 02138, USA

Received: 11 July 1998 / Accepted: 22 September 1998 / Published online: 17 December 1998

Abstract. To compare different implicit solvent potentials, the folding thermodynamics of the helical peptide RN24 and the β-hairpin peptide BH8 are studied by molecular dynamics simulation with adaptive umbrella sampling. As the potential energy functions, the analytical continuum solvent (ACS) potential and three simplified variants, termed $EPSR_1$, $EPSR_4$, and $EPSR_{10}$, are used. The ACS potential is a combination of the standard CHARMM force field for the internal energy (bonds, angles, dihedrals) and the van der Waals energy with the analytical continuum electrostatic (ACE) potential and a non-polar solvation potential. The EPSR potentials differ from the ACS potential by the use of Coulomb's law with a distance-dependent dielectric function to calculate the electrostatic energy. With the ACS potential, quantitative agreement with experiment is obtained for the helix propensity (RN24: 62% calculated vs 50–60% experiment) and the β-hairpin propensity (BH8: 33% calculated vs 19–37% experiment) of the peptides. During the simulations with the EPSR potentials, no significant formation of secondary structure is observed. It is shown that the preference for coil conformations over conformations with secondary structure by the EPSR potentials is due to an overestimation of the energy of salt bridge formation, independent of the magnitude of the Coulomb energy relative to the other energy terms. Possible improvements of the distance-dependent dielectric functions which may permit their application to the simulation of peptide folding, are discussed.

Key words: Helical peptide – β-Hairpin – Random coil – Umbrella sampling – Multicanonical sampling

1 Introduction

The structural characterization of peptides has been the subject of numerous experimental [1–9] and theoretical [10–19] studies. While many peptides are of interest because of their biological function, e.g., hormones, venoms, and anti-bacterial drugs, others have been studied to understand the principles governing secondary structure formation and processes that are thought to play a role in the initial stages of protein folding [20–24]. Circular dichroism (CD) and nuclear magnetic resonace (NMR) have shown that a number of peptides adopt a helical or β-hairpin structure in aqueous solution with significant probability, ranging from 20% to approximately 80% for the most structured peptides known to date [1, 5].

One important problem in theoretical studies of peptide structure is the requirement to account for the competition between solute-solvent and solute-solute interactions; e.g., when considering the helix-coil transition of a peptide, there are intramolecular hydrogen bonds formed in the helix, and solute-solvent hydrogen bonds in the coil state. In recent years, most simulation studies have, therefore, been performed with an explicit representation of water molecules surrounding the peptide, thus limiting the simulation time (on the order of 1 ns) and the number of transitions between different conformations. In many cases, simulations have been restricted to the high-temperature unfolding of a structured peptide conformation [10, 13, 14]. To reduce the computational cost of peptide and protein simulations in aqueous solution, several simplified treatments of the solvent have been proposed, e.g., solvent-accessible surface area or volume models with atomic or group solvation parameters [16, 25–30], mirror charges to account for the polarization of water [31, 32], and an effective energy function for the backbone dihedral angles [33, 34]. In a recent study of the C-peptide of ribonuclease A, Hansmann and Okamoto [18] used a vacuum potential with an explicit hydrogen-bonding term and a distance- dependent dielectric function to

*Contribution to the Proceedings of Computational Chemistry and the Living World, April 20–24, 1998, Chambery, France

Correspondence to: M. Schaefer
e-mail: schaefer@brel.u-strasbg.fr

account qualitatively for the solvent screening of charge interactions. Vacuum potentials of this type were widely used in the 1970s and 1980s, mostly because of limitations in the available computer power. Their use is justified in studies where the solvent plays only a minor role, e.g., when considering interactions in the interior of a protein, or studies of peptides and proteins where there are only minor structural changes. However, calculations of the secondary structure formation of peptides from random coil configurations necessarily involve large changes in the solvent accessibility of charged and polar groups, so that a more accurate treatment of (electrostatic) solvation is required.

Recently, we introduced an approach to compute the aqueous solution structures and thermodynamics of peptides which makes use of an implicit solvent potential and of umbrella sampling of the potential energy [19]. Good agreement with experiment was obtained for the thermodynamic properties (e.g., the equilibrium between the preferred secondary structure and the coil configurations) for several α-helical and β-hairpin peptides [35]. The analytical continuum solvent (ACS) potential employed in these studies includes the mean-field contribution of the aqueous solvent to the free energy of the system at a relatively low computational cost, i.e., compared to calculations of the same systems in vacuo, the calculation time is increased by only a factor of 4–5. The electrostatic term of the ACS potential is rigorously derived from the continuum electrostatic model and provides an approximation to the solution of the Poisson equation [36]. Adaptive umbrella sampling of the potential energy [37] was employed in the peptide studies because it is a very efficient means of searching for low-energy conformations. Moreover, it makes possible an estimate of the free energy differences between different types of structures, as well as the temperature-dependence of the observables, e.g., the secondary structure content [37–39].

In this work, we investigate the possibility of further simplifying the computational approach by using Coulomb's law with a distance-dependent dielectric function, $\epsilon(r)$, to calculate the electrostatic energy of the peptide in solution, instead of the continuum electrostatic free energy of the ACS potential. The modified potential energy function, referred to as "EPSR" (from EPSilon of R) in the following, is identical with the ACS potential except for the treatment of the electrostatic term. In particular, it includes the same non-polar solvation energy term as the ACS potential [19], which is similar to the widely used solvent-accessible surface approximations to the solvation free energy of apolar molecules [40–43] (see Theory and methods).

The energy terms of the ACS and EPSR potentials, and the method of umbrella sampling of the potential energy, are briefly reviewed in the Theory and methods section. In Results, the ACS and the EPSR potentials are applied to folding (umbrella sampling) simulations for two peptides: an analogue of the helical C-peptide of ribonucleas A termed RN24 (sequence: succinyl-AETAAAKFLRAHA-NH_2) [1], and the peptide BH8 (sequence: RGITVNGKTYGR) which has been designed to form a stable β-hairpin in solution [7]. The secondary structure contents at 275 K (the temperature of the experiments) calculated using the different potentials are compared with each other and with experiment. In the Discussion, the reasons for differences between the results obtained with the ACS and the EPSR potentials are analyzed and compared with the conclusions of Hansmann and Okamoto [18], who used an energy function similar to EPSR.

2 Theory and methods

For the molecular dynamics simulations, we use the ACS potential introduced by Schaefer et al. [19], and a potential termed EPSR which is identical except that Coulomb's law with a distance-dependent dielectric function is used for calculating the electrostatic energy. The two effective solvent potentials have the form

$$\text{ACS/EPSR:}\quad G^{\text{tot}}(\overline{x}) = E^{\text{intrn}}_{\text{solute}}(\overline{x}) + E^{\text{vdW}}_{\text{solute}}(\overline{x}) + G^{\text{np}}(\overline{x}) + G^{\text{el}}_{\text{X}}(\overline{x}) \tag{1}$$

where $E^{\text{intrn}}_{\text{solute}}$ and $E^{\text{vdW}}_{\text{solute}}$ are the standard internal (bond length, bond angles, dihedrals) and van der Waals energy of the CHARMM polar hydrogen potential energy function [44, 45], G^{np} is the non-polar solvation energy (see Sect. 2.3), and G^{el}_{X} is the electrostatic energy term (X = ACS or EPSR; see Sects. 2.1 and 2.2).

2.1 ACS electrostatic energy

The ACS electrostatic energy is calculated using the analytical continuum electrostatic (ACE) potential [36], which is an analytical approximation to the solution of the Poisson equation for the solute embedded in a dielectric continuum [46–48]. For a solute with n atoms and partial charges $q_1, \ldots, q_n$, the ACE energy is the sum of $n(n+1)$ self energy ($\propto q_i^2$) and $n(n-1)/2$ interaction energy ($\propto q_i q_j, i \neq j$) terms:

$$G^{\text{el}}_{\text{ACS}} = \sum_i G^{\text{self}}_{i0} + \sum_{i,k} G^{\text{self}}_{ik} + \sum_{i<j} G^{\text{int}}_{ij} \tag{2}$$

The first sum corresponds (up to a small correction due to the use of Gaussians to describe the atom volumes, instead of overlapping "hard spheres") to the Born self energy of the isolated atoms in aqueous solution, $G^{\text{self}}_{i0} \simeq q_i^2/2\epsilon_s R_i$ (ϵ_s, dielectric constant of the solvent; R_i, atom radius) [49]. The self energy potential G^{self}_{ik} accounts for the loss of electrostatic solvation of atom (charge) i due to the presence of atom (volume) k. For the electrostatic interaction between pairs of charges, G^{int}_{ij}, the generalized Born equation is used, which includes the Coulomb interaction between q_i and q_j and a screening term [50–52]. Since the solvent screening depends on the accessibility of the charges, the interaction energy G^{int}_{ij} is a function of the interatomic distance and of two parameters, b_i and b_j, termed the Born solvation radii of the atoms i and j. The Born radius of atom n is calculated by setting its solvation energy equal to that of an ion with radius b_n [49], which can be written in the form

$$b_n = \left(\frac{1}{\epsilon_s} - \frac{1}{\epsilon_i}\right)\frac{q_n^2}{2\Delta G_n^{self}} \tag{3}$$

where ϵ_i is the dielectric constant of the solute interior (see Sect. 2.5), and where ΔG_n^{self} is the atomic solvation energy, $\Delta G_n^{self} = G_{n0}^{self} - q_n^2/2\epsilon_i R_i + \sum_k G_{nk}^{self}$. Qualitatively, b_n of an atom n at the surface of the solute is on the order of the atom's van der Waals radius, R_n, whereas it is on the order of the molecular radius for atoms that are buried in the interior of the solute (for details, see [36]).

2.2 EPSR electrostatic energy

In the EPSR potential, Coulomb's law with a distance-dependent dielectric function, $\epsilon(r)$, is used for calculating the electrostatic energy of the solute:

$$G_{EPSR}^{el} = \sum_{i<j} \frac{q_i q_j}{\epsilon(r_{ij}) r_{ij}} \tag{4}$$

where r_{ij} is the distance between the atoms i and j. Three different choices for the dielectric function are studied which make use of the cubical switching function for the non-bonded cutoff in the CHARMM program [44]:

$$\mathrm{EPSR}_i (i = 1, 4, 10): \quad 1/\epsilon(r) = f_{sw}(r^2)/(1.4 \cdot i) \tag{5}$$

where

$$f_{sw}(r^2) = \begin{cases} (r_{off}^2 - r^2)^2 (r_{off}^2 + 2r^2)/r_{off}^6 & \text{if } 0 < r < r_{off}; \\ 0 & \text{if } r \geq r_{off}. \end{cases} \tag{6}$$

For the three dielectric functions, termed EPSR_1, EPSR_4, and EPSR_{10}, the cutoff parameter r_{off} is set equal to 8 Å. The general formula for the switching function in CHARMM is reduced to the form given in Eq. (6) if the distance r_{on}, where the switching begins, is set equal to 0 Å. The EPSR functions correspond, at least qualitatively, to distance-dependent dielectric functions that have been widely used in the past [53–57]. In particular, the parameters chosen for the function EPSR_1 (r_{on}, r_{off}, and the factor of 1.4) lead to a dielectric constant that is similar to the dielectric function of Ramstein and Lavery [57] in the distance range from 1 to 7 Å (see Fig. 1a). The dielectric functions EPSR_4 and EPSR_{10} are scaled with respect to EPSR_1 by factors of 4 and 10, respectively. At short distances (1.5–3 Å), the well-known distance-dependent dielectric function $\epsilon(r) = 4.5r$ [55, 56] yields Coulomb energies in the range between EPSR_4 and EPSR_{10}; for distances between 3 and 6 Å, it is similar to EPSR_{10}. The distance-dependent dielectric function proposed by Mehler [54, 58], which has been applied with some success in simulation studies of native protein structures, is very similar to the function $\epsilon(r) = 4.5r$ in the distance range from 1.5 to 10 Å (not shown). Both the dielectric function of Ramstein and Lavery [57] and the function of Mehler [54] are sigmoidal (though the deviation from linearity is small for $r \leq 10$ Å) and approach asymptotically the dielectric constant of bulk water in the long range

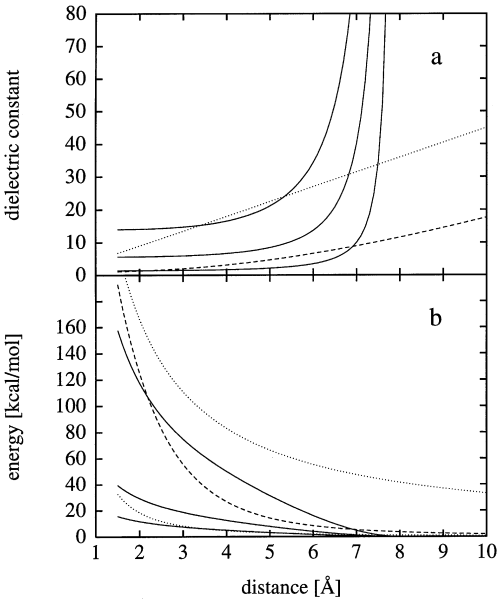

Fig. 1. **a** Dielectric constant as a function of distance, including the effect of the switching cutoff (EPSR functions). *Dotted line*: $\epsilon(r) = 4.5r$ (no cutoff); *dashed line*: dielectric function of Ramstein and Lavery [57] (no cutoff); *continuous lines*, from bottom: EPSR_1, EPSR_4, and EPSR_{10} [see Eq. (5)]. **b** Interaction energy of two unit charges as a function of distance, calculated using Coulomb's law, Eq. (4), and different distance-dependent dielectric functions and cutoff schemes. Line types same as in **a**, with the addition of the *upper dotted line*: constant $\epsilon(r) = 1$ (no cutoff); *continuous lines*, from top: EPSR_1, EPSR_4, and EPSR_{10}

($r \gg 10$ Å). This is not the case for the EPSR dielectric functions. From Fig. 1b, however, the differences between the Coulomb energies calculated using the different dielectric functions are small for distances $\geq$8 Å, despite the fact that the EPSR dielectric functions diverge at $r = 8$ Å (see also the Discussion). Note that the divergence of the EPSR dielectric functions is merely a consequence of the fact that the Coulomb energy of the EPSR potentials smoothely approaches 0 kcal/mol at the cutoff distance of 8 Å. Since the function EPSR_{10} yields very small energies at all distances, it makes it possible to study the dynamics of the peptides with the electrostatic interaction essentially turned off.

2.3 Non-polar solvation energy

The non-polar solvation energy term, G^{np}, in Eq. (1) is an approximation to the solvation free energy of the hypothetical uncharged solute [19]; it is given by a sum of atomic contributions:

$$G^{np}(\bar{x}) = \sum_i G_i^{np}(\bar{x}) = 4\pi\sigma \sum_i (R_i + R_s)^2 \frac{R_i}{b_i} \tag{7}$$

where R_i and R_s are the radius of atom i and of a water probe sphere, respectively, and b_i is the Born solvation radius of atom i (see Sect. 2.1). The quantity $4\pi(R_i + R_s)^2$ is the solvent-accessible surface of the isolated atom i. The proportionality of the non-polar solvation free energy of an atom to R_i/b_i is consistent

with the fact that the Born radius of an atom at the surface (in the interior) is small and on the order of R_i (large and on the order of the molecular radius; see Sect. 2.1). Despite the computational simplicity of the formula for the non-polar solvation energy, Eq. (7), it yields results that are very similar to those obtained with a solvent-accessible surface area model [59].

2.4 Multicanonical sampling

To search efficiently for low-energy conformations during the molecular dynamics simulations, we employ the method of multicanonical sampling [37–39] where an adaptive umbrella potential, U_n, is added to the potential energy:

$$G_n^{\mathrm{tot}^*} = G^{\mathrm{tot}} + U_n(G^{\mathrm{tot}}) \tag{8}$$

During the simulations, the umbrella potential $U_n(G^{\mathrm{tot}})$ is updated at regular intervals (in this work: every 10 ps) based on the statistics for the total energy G^{tot} from the time simulated thus far, using the weighted histogram analysis method (WHAM) equations [60–62]. The umbrella potential is determined such that in the limit of long simulation times, low and high potential energies G^{tot} are sampled with equal probability. Multicanonical sampling enables the system to overcome energy barriers between low-energy conformations and to explore conformation space with high efficiency, relative to a molecular dynamics simulation for the unmodified potential G^{tot} at constant temperature. Further advantages of the method are that it makes it possible to calculate canonical ensemble averages for a range of temperatures from a single trajectory, and that the density of states as a function of the potential energy can be derived from the converged umbrella potential. This makes possible calculation of the thermodynamics of the system (e.g., the free energy difference between the various states). For details of the methodology and its application to the simulation of peptides, see [37] and [19]; a discussion of some aspects of the method is given in the accompanying paper [63].

2.5 Simulation setup and parameters

The peptide simulations reported in Results start from the fully extended structure (all backbone and sidechain dihedral angles set equal to 180°, except for χ_2 of Phe, Tyr: 90°; and χ_2 of His: −90°). Gaussian-distributed velocities were assigned to the atoms at random, i.e., there is no bias toward a given (secondary) structure included in the initial conditions. The standard parameters of the polar-hydrogen (united atom) parameter set param19 of CHARMM are used [44, 45]. For the calculations with the ACS potential, the parameter set is augmented by the effective atom volumes of the atom types [19, 36], and by a "smoothing parameter" $\alpha = 1.2$ which yields best agreement between the solute volume description of the ACS potential (a superposition of atomic Gaussians with width $\sigma_i = \alpha R_i$, where R_i is the van der Waals radius) and the continuum model (a heavyside function which is equal to 1 in the solute interior, and 0 outside) [47, 64]. The atomic polarizability of the solute is assumed to be effectively included in the partial charges, in consistency with the derivation of the force-field parameters of CHARMM [44, 65], i.e., the solute interior is assigned a dielectric constant of $\epsilon_{\mathrm{i}} = 1$ in the ACE electrostatic potential. The solvent dielectric constant is set equal to $\epsilon_{\mathrm{s}} = 80$. Since the non-polar solvation term, G^{np}, is defined as the solvation free energy of the hypothetical uncharged solute, where differences between the contributions from apolar and polar atoms are expected to be small, we use a single parameter $\sigma = 3$ cal/(mol Å^2) for all atom types [19]. The value assigned to σ leads to a dependence of G^{np} on the solvent accessible surface corresponding to a "conventional" atomic solvation parameter of approximately 8 cal/(mol Å^2), a value that is in accord with solvation free energy data on small apolar molecules [66] and the analysis of the non-polar solvation free energy of small compounds by Still et al. [52]. In the calculations with the ACS potential, a switching cutoff from 8 to 12 Å is used. For consistency between the electrostatic energy and the van der Waals energy, and for computational efficiency, the same switching cutoff from 0 to 8 Å is used in the EPSR potentials. With respect to the short-ranged van der Waals energy, this is expected to make only a small difference relative to the use of an 8 to 12 Å switching cutoff. For the electrostatic energy, the switching-off from 0 to 8 Å is an essential part of reproducing qualitatively the screening behavior of distance-dependent dielectric functions (see Sect. 2.2 and the Discussion).

3 Results

Molecular dynamics trajectories over 6 ns with umbrella sampling of the potential energy were performed for the peptides RN24 [1] and BH8 [7], using the ACS potential and the potentials EPSR_1, EPSR_4, and EPSR_{10} (see Theory and methods). The peptide RN24 was shown experimentally (NMR and CD spectra) to adopt 50–60% helical conformations at $T = 275$ K [1, 67, 68]; the peptide BH8 was designed to form a β-hairpin in aqueous solution (19–37%, depending on the criterion and experimental approach [7]). Owing to the use of the umbrella sampling technique, the total energy, Eq. (1), varies during the simulations over a range of 350 kcal/mol, corresponding to ensembles of the peptide systems at temperatures ranging from 250 to 1100 K [37]. Figures 2 and 3 show the total energy, the helix content, and the degree of β-hairpin formation during the simulations with the ACS and the EPSR_1 potentials. To calculate the helix and hairpin content of a conformation, we used the program DSSP [69], which determines the secondary structure of a polypeptide based on hydrogen bond patterns. From the number of residues reported by DSSP as "helix" (N_{h}) and "antiparallel-β" (N_β), the helix and the hairpin contents are defined as $P_{\mathrm{h}} = N_{\mathrm{h}}/N_{\mathrm{res}}$ and $P_\beta = (N_\beta + 2)/N_{\mathrm{res}}$, if $N_\beta > 0$ ($P_\beta = 0$ if $N_\beta = 0$), where N_{res} is the total number of residues. For calculating the β-hairpin content with $N_\beta > 0$, we added

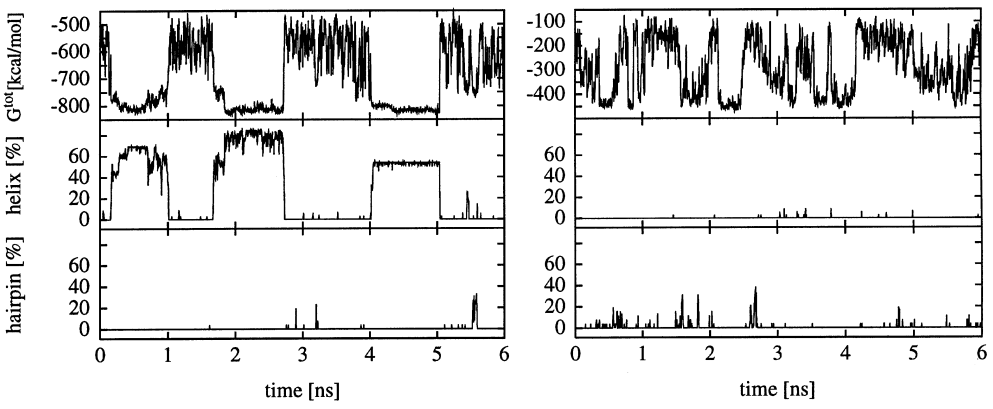

Fig. 2. Peptide RN24. *Left*: simulation with the ACS potential, Eqs. (1) and (2); *right*: simulation with the $EPSR_1$ potential, Eqs. (1) and (4). *Top*: total energy; *middle*: helix content; *bottom*: antiparallel-β content (averages over 4 ps intervals). Secondary structure calculated using the program DSSP [69] (see text)

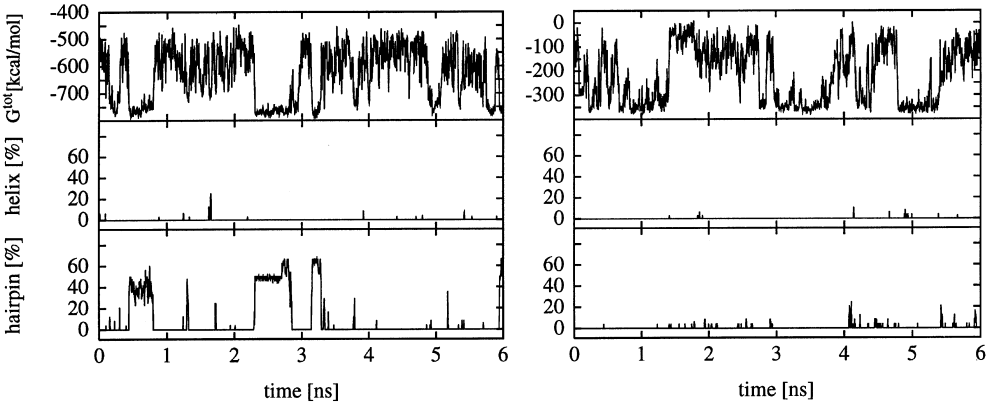

Fig. 3. Peptide BH8. *Left*: simulation with the ACS potential, Eqs. (1) and (2); *right*: simulation with the $EPSR_1$ potential, Eqs. (1) and (4). *Top*: total energy; *middle*: helix content; *bottom*: antiparallel-β content (averages over 4 ps intervals). Secondary structure calculated using the program DSSP [69] (see text)

2 to the number of antiparallel-β residues reported by DSSP to account for the turn between the two strands, which requires at least two residues, and which constitutes an integral part of the β-hairpin structure.

From Figs. 2 and 3, there are several instances during the simulations with the ACS potential where the peptides adopt the secondary structure observed in experiments (helix for RN24, β-hairpin for BH8) for periods of 0.5–1 ns. The non-native secondary structure occurs only for short periods of time and to a much smaller degree (up to ~35%, as compared with up to ~80% for the native secondary structure). By contrast, during the molecular dynamics simulations with the $EPSR_1$ potential, neither the native nor the non-native secondary structure is adopted by the peptides at a significant level. This difference is found in spite of the fact that the variations in the total energy during the simulations are of the same magnitude for the ACS and the $EPSR_1$ potentials (~350 kcal/mol), which indicates that low- and high-energy conformations are sampled efficiently in both cases.

To analyze the effect of using the ACS and $EPSR_1$ potentials, the difference between the maximum and the minimum of the energy terms in Eq. (1) were calculated from the simulations. From Table 1, the variations of the total energy and of the internal energy, E^{intrn}, are very similar for the ACS potential and the $EPSR_1$ potential (see also Figs. 2 and 3). The maximum changes of the van der Waals energy, E^{vdW}, and the non-polar solvation energy, G^{np}, are smaller for $EPSR_1$ than for ACS (reductions by 30% and 50%, respectively). By contrast, the maximum change in the electrostatic energy, G^{el}, of $EPSR_1$ is about 2.5 times larger than for the ACS potential. Furthermore, the maximum change in the Coulomb energy of $EPSR_1$ during the simulation is significantly larger than the change of E^{vdW} and G^{np} combined (i.e., the remaining non-bonded energy terms), whereas the contrary is the case for the ACS potential. Interestingly, the two terms of the electrostatic energy in the ACS potential, G^{self} and G^{int} (see Sect. 2.1), both vary over ranges of approximately 325 kcal/mol (RN24) and 260 kcal/mol (BH8), while their sum, G^{el}, changes over only 64 kcal/mol and only 66 kcal/mol. This is a consequence of the anticorrelation between G^{self} and G^{int}, i.e., of the competition between the electrostatic solvation of single charges (self energy or "charge-solvent" energy) and the favorable interaction between charge pairs [36].

The data summarized in Table 1 suggest that one reason for the failure of the simulations with the $EPSR_1$ potential to yield low-energy structures with secondary structure may be that the differences between the electrostatic energies of structures, relative to differences in E^{vdW} and G^{np}, are somewhat overestimated. To test this hypothesis, we performed umbrella sampling simulations for the RN24 and BH8 peptides with the $EPSR_4$ and $EPSR_{10}$ potentials, where the Coulomb energy is scaled by factors of 1/4 and 1/10 relative to that of $EPSR_1$ (see Sect. 2.2). As expected, the use of the $EPSR_4$ and $EPSR_{10}$ potentials leads to reduced ranges for the

Table 1. Energy ranges during umbrella sampling calculation[a]

Peptide	RN24				BH8			
	ACS	$EPSR_1$	$EPSR_4$	$EPSR_{10}$	ACS	$EPSR_1$	$EPSR_4$	$EPSR_{10}$
E^{intrn}	392.9	361.8	378.0	375.8	365.4	356.3	356.9	366.5
E^{vdW}	112.6	82.0	95.0	93.4	79.7	68.6	96.1	89.1
G^{np}	7.9	4.2	5.5	6.2	6.1	4.4	5.3	5.5
G^{self}	315.2	–	–	–	255.1	–	–	–
G^{int}	333.1	–	–	–	262.9	–	–	–
G^{el}	63.7	151.6	64.7	30.3	66.4	125.4	56.8	26.8
G^{tot}	461.5	459.7	457.0	461.8	426.0	438.9	438.5	440.9

[a] Difference between maximum and minimum of energy term during simulation (kcal/mol). For definition of ACS and EPSR potentials (column labels), see Sect. 2. Row labels: E^{intrn}, sum of internal energy terms; E^{vdW}, van der Waals energy; G^{np}, hydrophobic solvation, Eq. (7); G^{self}, self terms $\propto q_i^2$ in Eq. (2); G^{int}, interaction terms $\propto q_i q_j$ in Eq. (2); G^{el}, electrostatic free energy, Eq. (2) (ACS) or Coulomb energy (EPSR); G^{tot}, total energy, Eq. (1)

Table 2. Calculated secondary structure content at 275 K[a]

Peptide	RN24				BH8			
	ACS	$EPSR_1$	$EPSR_4$	$EPSR_{10}$	ACS	$EPSR_1$	$EPSR_4$	$EPSR_{10}$
Helix	62.29[b]	0.00	0.00	0.11	0.02	0.04	0.08	0.21
Hairpin	0.00	1.05	0.00	0.25	32.70[b]	0.01	0.07	0.42

[a] Canonical ensemble averages (see Sect. 2.4) over the trajectories calculated with the ACS and the EPSR potentials (values in %). Helix and antiparallel-β content calculated using the program DSSP [69]

[b] Numbers differ somewhat (58%, 38%, respectively) from those in Schaefer et al. [19], which are derived from another simulation (over 10 ns)

Coulomb energy during the simulations, though the reduction is by factors of $\sim$2 and 5 (see Table 1). This discrepancy with respect to the scaling of the Coulomb term in the potential is explained by the fact that the simulations with the $EPSR_4$ and $EPSR_{10}$ potentials lead to trajectories that are distinct from that obtained by simulation with $EPSR_1$. Despite the fact that during the simulations with $EPSR_4$ ($EPSR_{10}$), the maximum differences between the electrostatic energies of any two structures from the trajectories is similar to (smaller than) that for the simulations with the ACS potential, we found no significant formation of secondary structure, i.e., the results on helix and β-hairpin formation for $EPSR_4$ and $EPSR_{10}$ are qualitatively the same as for $EPSR_1$ (data not shown).

For a quantitative comparison, we calculated the secondary structure content of the peptides at the temperature of the experiments, $T = 275$ K, by evaluating canonical ensemble averages over the umbrella sampling trajectories (see Sect. 2.4 and [37]). From Table 2, there is good agreement between the helix content (RN24) and the β-hairpin content (BH8), calculated using the ACS potential, and experiment (RN24: 50–60% helix; BH8: 19–37% β-hairpin). As expected from Figs. 2 and 3, the secondary structure content from the simulation with the $EPSR_1$ potential is almost negligible ($<1\%$), both for the "correct" (experimental) and for the "misfolded" secondary structure (RN24: β-hairpin; BH8: helix). For the simulations with the $EPSR_4$ and $EPSR_{10}$ potentials, the results are similar, i.e., virtually no helical and β-hairpin structures contribute to the ensembles at 275 K.

To investigate the nature of the low-energy structures obtained from the simulations with the EPSR potentials, we displayed 10 structures from each trajectory which make the highest contribution to the ensembles at 275 K. For the ACS potential, the structures are all helical (RN24) and predominantly β-hairpin (BH8), consistent with the results in Table 2. For the EPSR potentials, the formation of a charge cluster involving charged sidechains (RN24: Glu2, Lys7, Arg10, His12; BH8: Arg1, Lys8, Arg12) and the chain termini (RN24: the negatively charged succinyl terminus; BH8: standard N- and C-termini) emerged as a feature that is common to all structures (Figs. 4 and 5). This suggests that it is the dominance of charge-charge interactions over the interaction of polar groups, in particular over the energetics of hydrogen bonds, which is responsible for the lack of secondary structure formation in the simulations with the EPSR potentials.

To quantify the magnitude of the contributions from charge-charge interactions and from interactions of the polar backbone of the peptide, we subdivided the atoms of the peptides in two groups: first, all sidechain atoms and the charged termini (see above), and second, the peptide backbone without the charged termini (i.e., the complement of the first group). The two groups are referred to as the "charged" (c) and the "backbone" (b) atom groups in the following. The sidechains of charged, polar, and apolar amino acids are included in the same group for simplicity; this is justified because the contribution of apolar and polar sidechains to the electrostatic energy is small compared with that of the charged sidechains.

For two atom groups, and independent of the potential that is considered, the total electrostatic energy, G^{el}_{tot}, can be written as the sum of three terms, the elec-

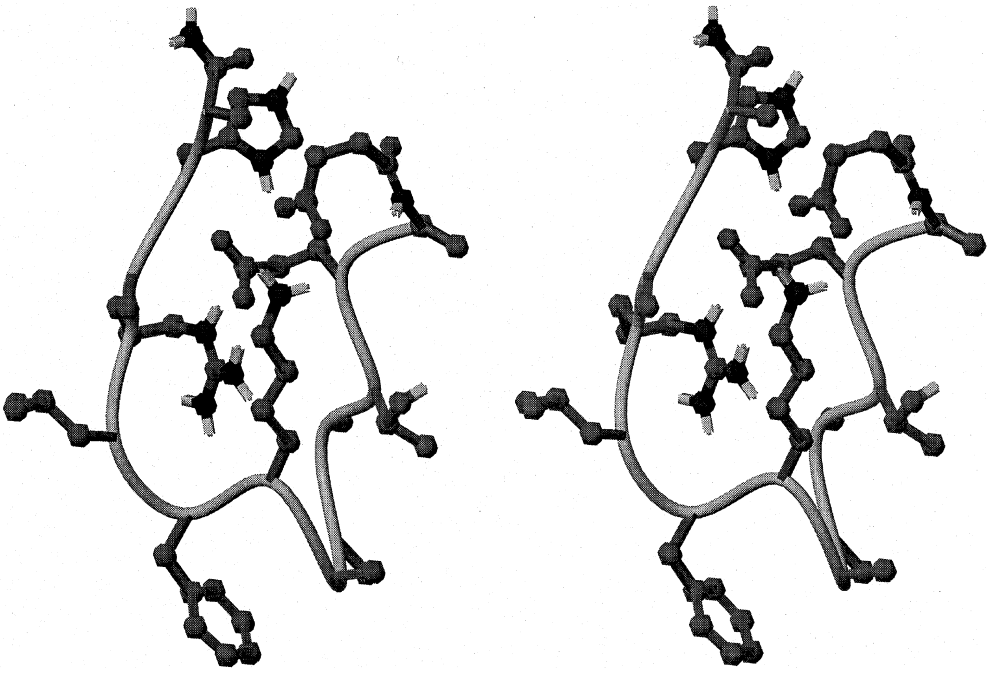

Fig. 4. Peptide RN24 at $t = 3.675$ ns of the simulation with the $EPSR_1$ potential (cross-eyed view). Succinyl (N) terminus in the top right corner. The charge cluster in the middle consists of a salt bridge succinyl–Lys7 (in the front) and the triad Arg10–Glu2–His12 (in the back)

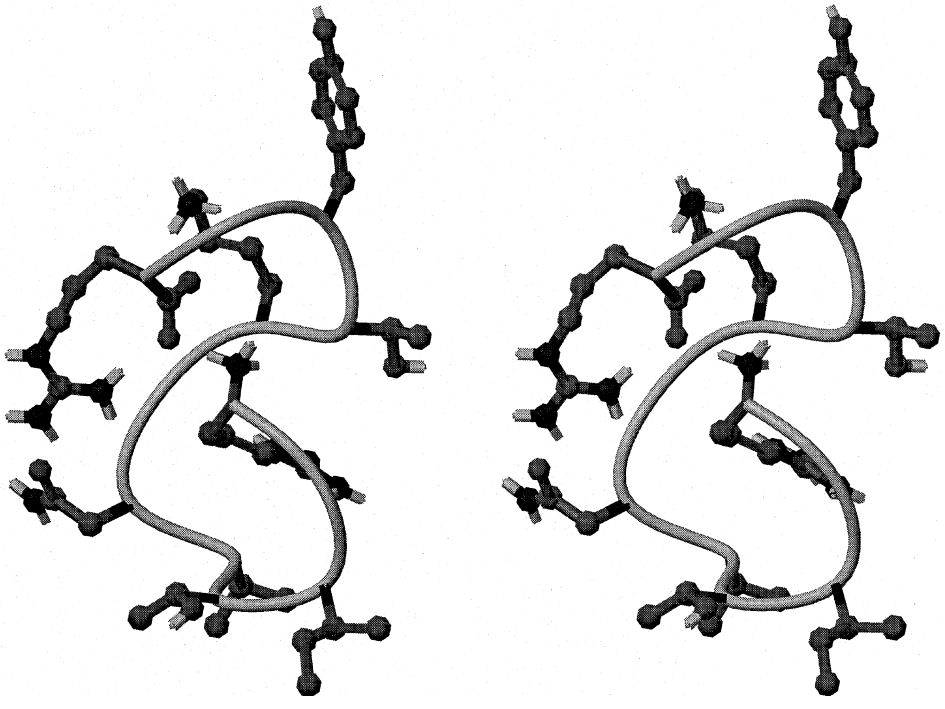

Fig. 5. Peptide BH8 at $t = 3.5815$ ns of the simulation with the $EPSR_1$ potential (cross-eyed view). C-terminus in the top left corner. The charge cluster consists of the C-terminus at the center of a triangle formed by the N-terminus, Lys8, and Arg12

trostatic energy of each separate group (i.e., the electrostatic energy with the atoms of the other group uncharged), and the electrostatic interaction between the groups (subscript "cb"):

$$G^{el}_{tot} = G^{el}_{c} + G^{el}_{b} + G^{el}_{cb} \tag{9}$$

As the reference state for analyzing the atom group contributions to G^{el} in the peptide RN24, we constructed an ideal α-helix by setting all ϕ/ψ dihedral angles to $-48°/-57°$ and all sidechain dihedral angles to 180° (except χ_2 of Phe, 90°, and His, $-90°$), followed by 50 steps of steepest descent minimization to eliminate bad contacts; for the minimization, the ACS potential was used. For the peptide BH8, a somewhat more complex procedure was used to construct a β-hairpin model. A total of 8 ps molecular dynamics were calculated using the ACS potential, starting with the fully extended chain at 1000 K and lowering the temperature to 600 K after 4 ps, and to 300 K after 6 ps. The extended chain was built by setting all backbone ϕ/ψ angles to $-140°/135°$; the dihedral angles of the strand residues (3–5 and 8–10) were kept fixed at these values during the dynamics. After every 2 ps, 100 steps of steepest descent minimization were performed. The formation of the β-hairpin

was induced by applying 4 NOE constraints on the distances between the peptide O and H atoms of the residues Ile3–Tyr10 and Val5–Lys8. In the final structure, the four restrained O—H distances were <2 Å, and the secondary structure analysis with the program DSSP [69] confirmed the formation of antiparallel β-strands for the residues 3–5 and 8–10. The end-to-end distance (from the N-terminal nitrogen to the C-terminal carbon atom) is 7.6 Å, i.e., the structure does not include a salt bridge between the chain termini. From the (ϕ/ψ) dihedral angles of Asn6 $(-57°/102°)$ and Gly7 $(80°/12°)$, it is evident that the strands are connected by a type II β-turn. The constructed "ideal" hairpin is thus in accord with the model of the β-hairpin proposed by Ramírez-Alvarado et al. [7], i.e., residues 3 through 10 form a β-hairpin while residues 1, 2 and 11,12 are pointing away from each other owing to electrostatic repulsion between Arg1 and Arg12. For the trajectories calculated with the ACS and EPSR potentials, we computed the group contributions to the electrostatic energy relative to their contributions in the ideal helix (RN24) and the ideal hairpin (BH8). For a given conformation at the simulation time t, the relative group contribution is then:

$$\Delta G_x^{\mathrm{el}}(t) = G_x^{\mathrm{el}}(t) - G_x^{\mathrm{el}}(\mathrm{ideal}) \tag{10}$$

where the subscript x refers to any of the energy terms in Eq. (9) (x = tot, c, b, cb).

Figure 6 shows the electrostatic energy and atom group contributions in RN24 relative to the helix. From a comparison with Fig. 2, the relative electrostatic energy, $\Delta G_{\mathrm{tot}}^{\mathrm{el}}$, of the ACS potential is positive for non-helical conformations (e.g., at $t = 1$–1.5 ns and $t = 3$–4 ns). For the ACS potential, the ideal helix is thus favored electrostatically over random coil structures. This is consistent with the fact that $\Delta G_{\mathrm{tot}}^{\mathrm{el}}$ is fluctuating around 0 kcal/mol (or it is a small negative energy, e.g., at $t \approx 2.2$ ns) at times when the RN24 peptide adopts a helical conformation. By contrast, the electrostatic energy for the $EPSR_4$ potential relative to that of the ideal helix is almost always negative, with a mean value of approximately -30 kcal/mol. This shows that the $EPSR_4$ potential qualifies coil structures (the helix and β-hairpin content of the RN24 peptide during the simulation with the $EPSR_4$ potential are insignificant; see Fig. 2 for the $EPSR_1$ potential, which yields similar results) as electrostatically more stable than the helical conformation. On top of the enthalpic destabilization by 5–40 kcal/mol due to the electrostatic energy, the helical state is expected to be entropically destabilized relative to the random coil state (even though it is rather structured, as in Fig. 4), which explains why the simulation with the $EPSR_4$ potential fails to produce helical peptide conformations.

From the atom group contributions in Fig. 6 it is possible to identify the origin of the different behavior of the ACS and the $EPSR_4$ electrostatic potential during the simulation. For both potentials, the relative contribution of the polar backbone, $\Delta G_{\mathrm{b}}^{\mathrm{el}}$, is positive, i.e., the ideal helix conformation is more stable than the conformations from the trajectories as far as the backbone is concerned. For $EPSR_4$, this is a direct consequence of the fact that the peptide does not form any secondary structure during the simulation, while the hydrogen bonds formed in the ideal helix are stabilizing because there is no competing charge-solvent interaction included in EPSR. The decrease in $\Delta G_{\mathrm{b}}^{\mathrm{el}}$ for the ACS potential at times where the peptide forms a helix (e.g., at $t \approx 0.5$ ns and $t \approx 2.2$ ns) reflects the formation of hydrogen bonds by the backbone. That $\Delta G_{\mathrm{b}}^{\mathrm{el}}$ is still on the order of 20 kcal/mol at times where the helix content is significant ($P_{\mathrm{helix}} > 60\%$, see Fig. 2) may be a consequence of several factors: first, the RN24 peptide forms only part of a helix during the simulation, whereas the ideal helix extends over the entire sequence; second, the energy of the helical reference state was calculated after an energy minimization of the structure, while the umbrella sampling calculation yields an ensemble of structures corresponding to a temperature range from 250 to 1000 K; and third, the helix formed during the simulation may consist of a mixture of residues in a 3_{10}, α, and π-helical conformation. The energetics of conversion between the different types of helices will be presented elsewhere [70].

With respect to the relative electrostatic energy of the charged atom group, $\Delta G_{\mathrm{c}}^{\mathrm{el}}$, the ACS and the $EPSR_4$ potentials behave very differently. For the ACS potential, $\Delta G_{\mathrm{c}}^{\mathrm{el}}$ is a small negative energy on the order of -3 kcal/mol, except at two instances where it is on the order of $+15$ kcal/mol (at $t = 3.2$ ns and $t = 4.3$–5 ns; see below). It follows that the energy of the charged atoms in the RN24 peptide is very similar for the ideal

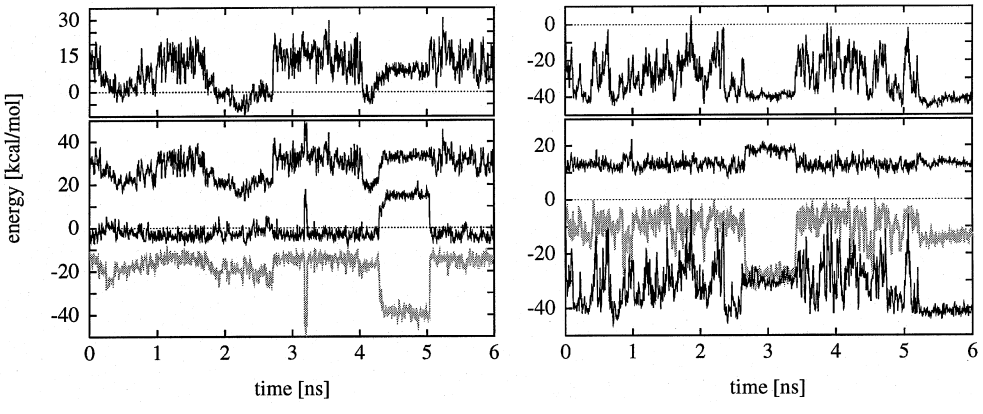

Fig. 6. Peptide RN24. Electrostatic energy of backbone/charged atom groups during the simulation, relative to the energy in the ideal helix (see text). *Left*: ACS potential; *right*: $EPSR_4$ potential. *Top*: total electrostatic energy, $G_{\mathrm{tot}}^{\mathrm{el}}$; *bottom*: contributions from the backbone, $G_{\mathrm{b}}^{\mathrm{el}}$ (*upper black curve*), the charged atom group, $G_{\mathrm{c}}^{\mathrm{el}}$ (*lower black curve*), and from the interaction between these atom groups, $G_{\mathrm{cb}}^{\mathrm{el}}$ (*gray curve*).

helix with extended sidechains and for most conformations that are sampled during the simulation, including random coil conformations. Since the energy of the atom group also includes the interaction between charged sidechains, this implies that the interaction of ionized groups is very effectively screened in the ACS potential. By contrast, ΔG_c^{el} is large and negative for almost all conformations during the simulation with the $EPSR_4$ potential; the mean and standard deviation are -32 ± 8 kcal/mol. Since there is only weak interaction between the sidechains in the ideal helix (the reference state), the large negative value of ΔG_c^{el} implies that there are strong charge-charge interactions present during the simulation with the $EPSR_4$ potential, which dominate the energetics and the conformational behavior of the system. This is consistent with the observation of charge clusters for all low-energy structures from the EPSR trajectories (see Figs. 4 and 5).

From a comparison of Figs. 2 and 6 for the ACS potential, there is weak stabilization of helical conformations of the RN24 peptide by the interaction between the backbone and charged atom groups, ΔG_{cb}^{el} (decrease of the interaction curve from approximately -15 kcal/mol for coil conformations to values in the range -20 to -25 kcal/mol at $t = 0.2$–1 ns and $t = 2$–3 ns). From the data, it is not possible to distinguish whether the favorable interaction between the backbone and the charged atoms involves the helical part of the backbone or the non-helical residues. However, from a visual inspection of the structures in the time interval $t = 4.3$–5 ns, where the peptide is 50% helical, we determined that the concurrent significant drop of the interaction energy to values of approximately -40 kcal/mol is due to the formation of hydrogen bonds between the non-helical part of the backbone (residues 1–5) with the carbonyl group of the succinyl terminus; the charged sidechains in the helical part of the peptide (residues 6–11, including Lys7, Arg10, and His12), as well as the sidechain of Glu2, extend out into the solvent and, consequently, do not contribute to the significant decrease of ΔG_{cb}^{el}. A similar occurrence of a structure where there are hydrogen bonds formed between a charged group and the peptide backbone is seen during the simulation with the $EPSR_4$ potential (see Fig. 6).

For the $EPSR_1$ and $EPSR_{10}$ potentials, the results on the group contributions to the electrostatic energy are qualitatively the same as for the $EPSR_4$ potential, i.e., the interaction energy of the charged sidechains and the succinyl terminus dominates over the energetics of hydrogen bond formation of the peptide backbone. In the case of the $EPSR_1$ potential, the energy of the charged atom group for coil structures is 150–200 kcal/mol lower than its energy in the ideal helix, while the interaction of the polar atom group (peptide N—H and C=O) in the helix yields only ~30 kcal/mol relative to the coil state. These results are in agreement with the fact that the $EPSR_4$ and $EPSR_{10}$ potentials are obtained from $EPSR_1$ by the scaling of the electrostatic contribution, and that the scaling does not change the relative order (i.e., importance) of the contributions from the atom groups.

For the atom group contributions to the electrostatic energy in BH8, we obtained results that are consistent with those for the peptide RN24. The electrostatic energy, relative to the energy of the ideal β-hairpin, is positive during the simulation with the ACS potential, i.e., it favors the structured state; it approaches 0 kcal/mol only at times where the peptide forms a β-hairpin (compare Figs. 3 and 7). By contrast, the relative electrostatic energy during the simulation with the $EPSR_4$ potential is in the range from -30 to 0 kcal/mol, thus favoring coil structures over the hairpin (compare Fig. 3 for the simulation with the $EPSR_1$ potential, which yields qualitatively similar results on the β-hairpin content during the simulation). The interaction between charged atom groups (charged sidechains and the chain termini) is responsible for the more favorable electrostatic energy of coil conformations. The relative energy of the charged group in the coil state is in the range from -10 to -30 kcal/mol; this is larger in magnitude than the energy gained by hydrogen bond formation in the β-hairpin, which is ~10 kcal/mol. As for RN24, the data on the group contributions to the electrostatic energy of BH8 for the potentials $EPSR_1$ and $EPSR_{10}$ are consistent with those obtained for $EPSR_4$ (not shown); for all EPSR potentials, the interaction of charged atom groups dominates the electrostatics of the BH8 peptide.

4 Discussion

The ACS potential and umbrella sampling of the potential energy within a molecular dynamics frame-

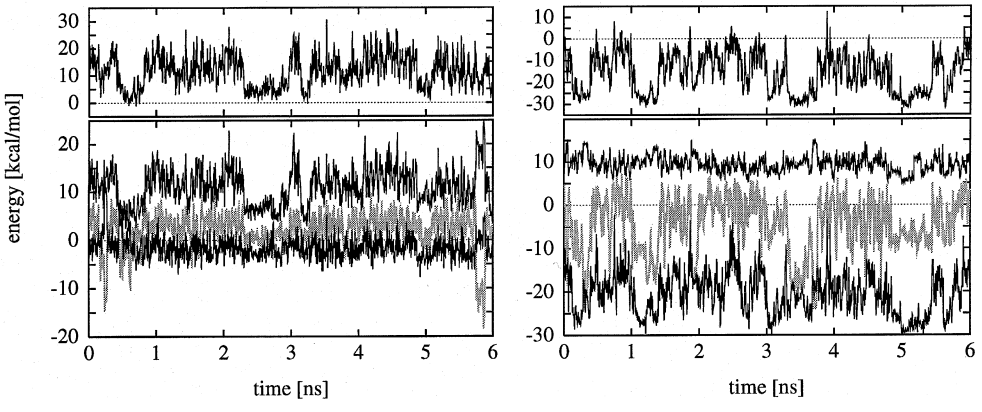

Fig. 7. Peptide BH8. Electrostatic energy of backbone/charged atom groups during the simulation, relative to the energy in the ideal β-hairpin (see text). *Left*: ACS potential; *right*: $EPSR_4$ potential. *Top*: total electrostatic energy, G_{tot}^{el}; *bottom*: contributions from the backbone, G_b^{el} (*upper black curve*), the charged atom group, G_c^{el} (*lower black curve*), and from the interaction between these atom groups, G_{cb}^{el} (*gray curve*)

work have been shown to yield a sequence-dependent secondary structure preference for the peptides RN24 (helix) and BH8 (β-hairpin), in quantitative agreement with experiment. By contrast, use of the potentials employing Coulomb's law with a distance-dependent dielectric function ($EPSR_1$, $EPSR_4$, and $EPSR_{10}$) did not lead to the formation of secondary structure during the simulations. With respect to the range of the energy terms that were sampled, the $EPSR_4$ potential has properties that are similar to the ACS potential; in particular, the energy range for the electrostatic term differs by only 2% (RN24) and 14% (BH8). The electrostatic energy ranges observed for the $EPSR_1$ and $EPSR_{10}$ potentials respectively, are considerably larger (by a factor of $\sim$2) and smaller (by a factor of $\sim$0.5) than that of the ACS potential. This indicates that neither an overestimation nor an underestimation of the electrostatic energy term in the EPSR potentials is responsible for the lack of secondary structure formation.

The switching cutoff of the EPSR Coulomb term in the distance range from 0 to 8 Å was introduced to reproduce, at least qualitatively, the screening behavior of distance-dependent dielectric functions known from the literature (see Fig. 1). Even though there are only small differences between the Coulomb energies for $r > 8$ Å calculated using the EPSR dielectric functions (which diverge at $r = 8$ Å) and sigmoidal dielectric functions [54, 57] (which have the correct limit of $\epsilon = 80$ in the long range), it is possible that the inclusion of electrostatic interactions beyond the 8 Å limit is required to induce the formation of secondary structure in molecular dynamics simulations. The inclusion of long-range electrostatic forces might be particularly important for helix formation, which involves the cooperative alignment of polar groups of the backbone along the helix axis. For example, the rise per helix turn in an α-helix is 5.6 Å [71], such that the calculations with the EPSR potentials include the interaction of backbone polar groups over approximately 1.4 helix turns, whereas the calculations with the ACS potential (12 Å cutoff) account for interactions over more than 2 helix turns.

From consideration of the electrostatic energy contributions of the backbone atoms and of the (charged) sidechains, it was shown that the formation of charge clusters during the simulations with the EPSR potentials is responsible for the preference of coil structures over helical/β-hairpin structures. Such charge interactions are weak in the presence of the ACS potential, as they are in explicit solvent. This is due to the fact that the electrostatic free energy as represented in the ACS potential is the sum of two contributions: the generalized Born term for charge-charge interaction and the charge-solvent (self-energy) term. It has been pointed out previously that the anticorrelation between these two terms leads to highly effective screening of charge-charge interactions in the interior of proteins [72]. The compensatory effect between the loss of individual charge solvation (self energy) and the energy gain due to charge-charge interaction is accounted for in the continuum electrostatic model and included in the ACS potential. However, the EPSR potentials only have weak screening of the charges and no charge solvation, so that the formation of charge clusters strongly stabilizes the denatured peptides during the simulations. Since the dominance of the energetics of ion pairs over that of hydrogen bonds is due to interactions at short range, the failure of the calculations with the EPSR potentials to yield stable secondary structure is independent of the cutoff used, i.e., the inclusion of long-range electrostatic interactions alone is not expected to improve the results that can be obtained from distance-dependent dielectric functions.

In a recent publication [73], the difference between the Coulomb energy with a distance-dependent dielectric function [$\epsilon(r)$, solvent] and the Coulomb energy in vacuum ($\epsilon = 1$) was interpreted as an electrostatic solvation energy and compared with the results from continuum electrostatic calculations. While such a comparison may be formally correct, it should be noted that distance-dependent dielectric functions are not designed to yield solvation free energies; instead, their introduction was motivated by their simplicity. It is justified in cases where there is little change in the solvent accessibility of charged and polar groups so that the reduction of the Coulomb interaction between charges due to solvation is most important. Examples where distance-dependent dielectric functions are applicable are processes in the interior of a protein, or the dynamics of small molecules where all atoms are exposed to the solvent. From the results presented in this work, we conclude that for a successful use of distance-dependent dielectric functions for simulating peptides and proteins, including structural changes, the following modifications should be considered:

1. A change of the functional form of the distance-dependent dielectric function, such that the energy of hydrogen bonds is increased relative to that of a charge-pair, i.e., the electrostatic potential should be more short ranged.
2. Use of the $EPSR_1$ potential with the charged groups neutralized.
3. Use of an explicit hydrogen bond potential in conjunction with a distance-dependent dielectric function with a large ϵ, e.g., the potential $EPSR_{10}$.

For the first option, it may be sufficient to use sigmoidal dielectric functions available from the literature [54, 57] with modified parameters such that the energy of salt bridge formation is reduced. The second option has been used successfully for protein unfolding simulations, where a distance-dependent dielectric function was combined with an occupied volume approximation for the solvation free energy [30]. The third option was employed in folding simulations of the RN24 peptide [18], which yielded good agreement with experiment. Since there is no desolvation contribution to the electrostatic energy of charged and polar groups in an apolar environment, the $EPSR_1$ potential may yield more meaningful results in that case. Thus, the structures for the two peptides with strong charge-charge interactions obtained in the EPSR simulations could exist in membranes, for example.

Acknowledgements. M.S. was supported in part by a research training grant within the Biotechnology programme of the Euro-

pean Community. C.B. was supported by the EMBO long-term fellowship ALTF 448-1995 and the fellowship 823A-050424 of the Swiss National Science Foundation. The Laboratory is supported in part by the CNRS (ISIS-UPRESA 7006 CNRS), by the Ministère de l'Education Nationale, by a grant from the Association pour la Recherche contre le Cancer (France), and by a grant from the National Institutes of Health (USA).

References

1. Osterhout JJ Jr, Baldwin RL, York EJ, Stewart JM, Dyson HJ, Wright PE (1989) Biochemistry 28:7059
2. Scholtz JM, York EJ, Stewart JM, Baldwin RL (1991) J Am Chem Soc 113:5102
3. Jao J, Dyson HJ, Wright PE (1994) J Mol Biol 243:754
4. Blanco FJ, Rivas G, Serrano L (1994) Nat Struct Biol 1:584
5. Searle MS, Williams DH, Packman LC (1995) Nat Struct Biol 2:999
6. Friedrichs MS, Stouch T, Bruccoleri RE, Mueller L, Constantine KL (1995) J Am Chem Soc 117:10855
7. Ramírez-Alvarado M, Blanco FJ, Serrano L (1996) Nat Struct Biol 3:604
8. Ni F, Carpenter KA, Ripoll DR, Sanderson SD, Hugli TE (1996) Biopolymers 38:31
9. Blanco F, Ramírez-Alvarado M, Serrano L (1998) Curr Opin Struct Biol 8:107
10. Tirado-Rives J, Jorgensen W (1991) Biochemistry 30:3864
11. Smith PE, Pettitt BM (1991) J Am Chem Soc 113:6029
12. Tirado-Rives J, Maxwell DS, Jorgensen WL (1993) J Am Chem Soc 115:11590
13. Hirst JD, Brooks CL III (1995) Biochemistry 34:7614
14. Pugliese L, Prévost M, Wodak SJ (1995) J Mol Biol 251:432
15. Hempel JC, Fine RM, Hassan M, Ghoul W, Guaranga A, Koerber SC, Li Z, Hagler AT (1995) Biopolymers 36:283
16. Wang L, O'Connell T, Tropsha A, Hermans J (1996) Biopolymers 39:479
17. Constantine KL, Friedrichs MS, Stouch TS (1996) Biopolymers 39:591
18. Hansmann UHE, Okamoto Y (1998) J Phys Chem 102:653
19. Schaefer M, Bartels C, Karplus M (1998) J Mol Biol 284:835
20. Wright PE, Dyson HJ, Lerner RA (1988) Biochemistry 27:7167
21. Itzhaki LS, Neira JL, Ruiz-Sanz J, de Prat Gay G, Fersht AR (1995) J Mol Biol 254:289
22. Yang JJ, Buck M, Pitkeathly M, Kotik M, Haynie DT, Dobson CM, Radford SE (1995) J Mol Biol 252:483
23. Blanco FJ, Serrano L (1995) Eur J Biochem 230:634
24. Muñoz V, Thompson PA, Hofrichter J, Eaton WA (1997) Nature 390:196
25. Gibson KD, Scheraga HA (1967) Proc Natl Acad Sci USA 58:420
26. Wesson L, Eisenberg D (1992) Protein Sci 1:227
27. Schiffer CA, Caldwell JW, Stroud RM, Kollman PA (1992) Protein Sci 1:396
28. Fraternali F, van Gunsteren WF (1996) J Mol Biol 256:939
29. Sung S-S, Wu X-W (1996) Proteins Struct Funct Genet 25:202
30. Lazaridis T, Karplus M (1997) Science 278:1928
31. Schaefer M, Froemmel C (1990) J Mol Biol 216:1045
32. Abagyan R, Totrov M (1994) J Mol Biol 235:983
33. Pedersen JT, Moult J (1997) J Mol Biol 269:240
34. Sartori F, Melchers B, Böttcher H, Knapp EW (1998) J Chem Phys 108:8264
35. Schaefer M, Bartels C, Karplus M (1998) in preparation
36. Schaefer M, Karplus M (1996) J Phys Chem 100:1578
37. Bartels C, Karplus M (1998) J Phys Chem B 102:865
38. Hansmann UHE, Okamoto Y, Eisenmenger F (1996) Chem Phys Lett 259:321
39. Nakajima N, Nakamura H, Kidera A (1997) J Phys Chem 101:817
40. Hermann RB (1972) J Phys Chem 76:2754
41. Chothia C (1974) Nature 248:338
42. Amidon GL, Yalkowsky SH, Anik ST, Valvani SC (1975) J Phys Chem 79:2239
43. Ooi T, Oobatake M, Némethy G, Scheraga HA (1987) Proc Natl Acad Sci USA 84:3086
44. Brooks BR, Bruccoleri RE, Olafson BD, States DJ, Swaminathan S, Karplus M (1983) J Comput Chem 4:187
45. Neria E, Fischer S, Karplus M (1996) J Chem Phys 105:1902
46. Kirkwood JG (1934) J Chem Phys 2:351
47. Davis ME, McCammon JA (1990) Chem Rev 90:509
48. Honig B, Nicholls A (1995) Science 268:1144
49. Born M (1920) Z Phys 1:45
50. Klopman G (1967) Chem Phys Lett 1:200
51. Constanciel R, Contreras R (1984) Theor Chim Acta 65:1
52. Still WC, Tempczyk A, Hawley RC, Hendrickson T (1990) J Am Chem Soc 112:6127
53. McCammon JA, Wolynes PG, Karplus M (1979) Biochemistry 18:927
54. Mehler EL, Eichele G (1984) Biochemistry 23:3887
55. Weiner SJ, Kollman PA, Nguyen DT, Case DA (1986) J Comput Chem 7:230
56. Pickersgill RW (1988) Protein Eng 2:247
57. Ramstein J, Lavery R (1988) Proc Natl Acad Sci USA 85:7231
58. Solmajer T, Mehler EL (1991) Protein Eng 4:911
59. Schaefer M, Bartels C, Karplus M (1998) in preparation
60. Ferrenberg AM (1989) PhD thesis, Carnegie-Mellon University
61. Kumar S, Bouzida D, Swendsen RH, Kollman PA, Rosenberg JM (1992) J Comput Chem 13:1011
62. Bartels C, Karplus M (1997) J Comput Chem 18:1450
63. Bartels C, Schaefer M, Karplus M (1998) DOI 10.1007/s00214980m144
64. Harvey SC (1989) Proteins Struct Funct Genet 5:78
65. MacKerell AD Jr, et al (1998) J Phys Chem 102:3586
66. Abraham MH (1982) J Am Chem Soc 104:2085
67. Kim PS, Baldwin RL (1984) Nature 307:329
68. Shoemaker KR, Kim PS, York EJ, Stewart JM, Baldwin RL (1987) Nature 326:563
69. Kabsch W, Sander C (1983) Biopolymers 22:2577
70. Bartels C, Schaefer M, Karplus M (1998) in preparation
71. Schulz GE, Schirmer RH (1978) Principles of protein structure. Springer, Berlin Heidelberg New York
72. Warshel A, Russell ST (1984) Q Rev Biophys 17:283
73. Edinger SR, Cortis C, Shenkin PS, Friesner RA (1997) J Phys Chem 101:1190